

# Kilohertz quasi-periodic oscillations in neutron-star X-ray binaries: flattening of the lag spectrum with increasing luminosity

Valentina Peirano   and Mariano Méndez

*Kapteyn Astronomical Institute, University of Groningen, PO Box 800, NL-9700 AV Groningen, the Netherlands*

Accepted 2021 June 29. Received 2021 June 17; in original form 2021 February 16

## ABSTRACT

We study the energy-dependent time lags and rms fractional amplitude of the kilohertz quasi-periodic oscillations (kHz QPOs) of a group of neutron-star low-mass X-ray binaries. We find that for the lower kHz QPO both the slope of the best-fitting linear model to the time-lag spectrum and the total rms amplitude integrated over the 2–25 keV energy band decrease exponentially with the luminosity of the source. For the upper kHz QPO, the slope of the time-lag spectrum is consistent with zero, while the total rms amplitude decreases exponentially with the luminosity of the source. We show that both the slope of the time-lag spectrum and the total rms amplitude of the lower kHz QPO are linearly correlated with a slope of  $\sim 1$ . Finally, we discuss the mechanism that could be responsible for the radiative properties of the kHz QPOs, with the variability originating in a Comptonizing cloud or corona that is coupled to the innermost regions of the accretion disc, close to the neutron star.

**Key words:** accretion, accretion discs – stars: neutron – X-rays: binaries.

## 1 INTRODUCTION

Quasi-periodic oscillations (QPOs) are variability features observed in the power spectra of neutron-star and black-hole low-mass X-ray binaries (LMXBs; Strohmayer et al. 1996; van der Klis et al. 1996; Morgan, Remillard & Greiner 1997; Strohmayer 2001). The oscillations detected at the highest frequencies in the power density spectra of LMXBs are called kilohertz QPOs (kHz QPOs; see Méndez & Belloni 2020, for a review). In neutron-star LMXBs, kHz QPOs are sometimes observed in pairs and, depending on their central frequency, are called the lower and the upper kHz QPOs. Besides these high-frequency features, the power spectra of LMXBs have a plethora of different types of variability and a noise component, known as broad-band noise (BBN), at lower frequencies (see e.g. Belloni, Psaltis & Klis 2002, for a description of variability features in the power spectra of LMXBs).

Variability in LMXBs is usually fitted using a sum of Lorentzian functions that describe the shape of the power spectrum of a source (e.g. Miyamoto et al. 1991; Grove et al. 1994; Berger & van der Klis 1998; Nowak 2000; van Straaten et al. 2002; Pottschmidt et al. 2003). These Lorentzian functions are characterized by three parameters: the central frequency,  $\nu_0$ ; the quality factor,  $Q = \nu_0/\text{FWHM}$ , where FWHM is the full width at half-maximum; and the integral of the power under the Lorentzian function. These properties allow us to identify kHz QPOs, with  $\nu_0$  ranging from 250 to 1300 Hz, and differentiate the lower component from the upper component. The quality factor (Barret, Olive & Miller 2005b; Peille, Barret & Uttley 2015) and the rms amplitude (Di Salvo et al. 2001; Méndez, van der Klis & Ford 2001), for example, behave differently for the lower and

the upper kHz QPO. In particular, for the lower kHz QPO, the rms amplitude first increases and then decreases with increasing QPO frequency (see e.g. van Straaten et al. 2002; Barret, Olive & Miller 2006; Méndez 2006; Ribeiro et al. 2019), whereas the rms amplitude of the upper kHz QPO generally decreases with increasing QPO frequency (van Straaten et al. 2002; Méndez 2006; Altamirano et al. 2008; Troyer et al. 2018).

Another property of the QPO signal is the energy-dependent time (or phase) lag. In recent years, time lags have been used more often to study the properties of the physical components in the accretion flow that produce the variability in LMXBs (e.g. Vaughan et al. 1997; Kaaret et al. 1999; Barret 2013; de Avellar et al. 2013, 2016). Particularly for the lower kHz QPO, the time lags are generally soft (the soft/low-energy photons lag behind the hard/high-energy ones), ranging from  $\sim 15$  to  $\sim 40$   $\mu$ s between photons in the 3–8 keV band and those in the 8–30 keV band (Barret 2013; de Avellar et al. 2013). The time lags of the upper kHz QPO are hard (the hard/high-energy photons lag behind the soft/low-energy ones) for all energy bands and QPO frequencies, inconsistent with those of the lower kHz QPO (de Avellar et al. 2013; Peille et al. 2015).

Correlations derived from the properties of QPOs (see Uttley et al. 2014, for a review on timing techniques) have been subject of detailed study, as the QPO properties are believed to be closely related to phenomena occurring close to the neutron star or the black hole, at the innermost regions of LMXBs (see e.g. Miller, Lamb & Cook 1998b; van der Klis 2005; Psaltis 2008). Consequently, QPO properties are a unique tool to directly observe and measure effects that occur in extreme gravitational environments, as the ones in LMXBs. While the central frequency of kHz QPOs reveals the dynamical time-scales of the system (Strohmayer et al. 1996), the lags can be used to understand the radiative processes of the accretion flow at even shorter time-scales, closer to the compact object, revealing

\* E-mail: [v.peirano@astro.rug.nl](mailto:v.peirano@astro.rug.nl)

the radiative mechanism responsible for the variability in LMXBs (Lee & Miller 1998).

Multiple models have been developed throughout the years to try and explain the relations among the different properties of QPOs, and between these properties and the spectral evolution of the source or its mass accretion state. Most models focused their efforts in explaining the dynamical properties of the QPOs, exploring the mechanism that produces the QPO central frequencies (Stella & Vietri 1997; Miller, Lamb & Psaltis 1998a; Osherovich & Titarchuk 1999; Kluzniak & Abramowicz 2001; Titarchuk 2003). Models that explain the dependence of the  $Q$  factor on the central frequency of the QPO have been used less often to describe the nature of the variability (Barret et al. 2005b). Finally, models have been proposed to explain the dependence of the lags and rms amplitude on frequency and energy (Lee & Miller 1998; Lee, Misra & Taam 2001; Kumar & Misra 2014, 2016; Karpouzas et al. 2020).

Recently, Troyer et al. (2018) carried out a systematic study of the time lags, fractional rms amplitude, covariance, and coherence function of the lower and upper kHz QPOs in 14 different LMXBs. These authors observed that the time lags of the lower kHz QPOs were consistently soft on all sources and either decreased or remained more or less constant as the energy increases from  $\sim 3$  to 12 keV. On the contrary, for the upper kHz QPO the time lags were consistent with zero, with larger errors than for the lags of the lower kHz QPO. Troyer et al. (2018) concluded that this must mean that the mechanisms producing the lower and upper kHz QPOs are different in nature (see also de Avellar et al. 2013; Peille et al. 2015). Méndez (2006) studied the behaviour of the maximum quality factor and fractional rms amplitude of the kHz QPOs in 12 different LMXBs, and found that for both the lower and upper kHz QPOs the maximum fractional rms amplitude decreases exponentially with increasing luminosity of the source, while for the lower kHz QPOs the maximum coherence increases up to a certain luminosity and then decreases exponentially.

Motivated by these results, in this paper we explore the dependence of both the fractional rms amplitude and the time lags of the lower kHz QPOs in the LMXBs studied by Troyer et al. (2018) upon luminosity. In Section 2, we describe the data that we obtained from the literature. In Section 3, we show the results of the analysis of these data, and in Section 4 we discuss the implications of these results.

## 2 DATA SELECTION AND ANALYSIS

The data we use in this paper were collected with the *Rossi X-ray Timing Explorer* (RXTE; Bradt, Rothschild & Swank 1993), using the Proportional Counting Array (PCA; Jahoda et al. 1996), and taken from the analysis in Troyer et al. (2018). Using the full RXTE/PCA energy band, with a time resolution of at least 125  $\mu$ s, they analysed observations of 14 neutron-star LMXBs that showed either one or two kHz QPOs. Troyer et al. (2018) identified the lower and upper kHz QPOs in each observation using the criteria of Peille et al. (2015), based on the quality factor  $Q$  of the QPOs. They calculated the energy-dependent spectral timing products using the shift-and-add technique (Méndez et al. 1998) on both the power spectra and cross-spectra of all observations. Energy-dependent time lags were calculated in several narrow energy bands with respect to the full-reference band, and averaged over frequency across the FWHM of the Lorentzian function that describes the QPO (see figs 8 and 9 in Troyer et al. 2018). Broad-band lags were calculated as the average of the frequency-dependent time lags between two broad energy bands, 3–8 and 8–20 keV (see figs 6 and 7 in Troyer et al. 2018). In

the convention of Troyer et al. (2018), positive time lags represent ‘soft lags’, where the low-energy photons arrive after the high-energy photons to the detector (see Troyer et al. 2018, for more details about the analysis of the data).

When selecting the sources in our sample, we consider that both fractional rms amplitude (Di Salvo et al. 2001; Méndez et al. 2001; Barret et al. 2005b; Méndez 2006; Ribeiro et al. 2017, 2019) and lags (Barret 2013; de Avellar et al. 2013; Peille et al. 2015; de Avellar et al. 2016) of the lower kHz QPO depend on QPO frequency. Barret (2013) and de Avellar et al. (2013) showed, for example, that in both 4U 1608–52 and 4U 1636–53 the lag of the lower kHz QPO increases and then decreases with increasing QPO frequency. In fig. 1 in Troyer et al. (2018), it is apparent that from the 14 sources they analysed, only 8 have measurements covering the full range of frequencies of the lower kHz QPOs. As a consequence of the behaviour of the lag and the fractional rms amplitude with QPO frequency, averaging those quantities over all frequencies in the six sources from Troyer et al. (2018) that have sparse measurements in the frequency range of the QPO would lead to systematic errors in the analysis. Therefore, here we only study the eight sources (see Table 2) with data covering evenly the entire frequency range of the lower kHz QPO. In contrast, for the upper kHz QPO, the coverage in QPO frequency is not as critical, since the lags are constant with QPO frequency (see e.g. de Avellar et al. 2013; Peille et al. 2015). Hence, we also included in our sample the six sources where Troyer et al. (2018) identified the presence of upper kHz QPOs.

Once we defined our sample, we searched in the literature for the average luminosity of each source. For most sources we used the lower kHz QPO frequency of each source to read off the luminosity from fig. 1 in Ford et al. (2000), following Méndez (2006). For 4U 1702–43, we obtained the luminosity from fig. 4 in Jonker et al. (2001), using the fractional rms amplitude as input. In Ford et al. (2000) they estimated the luminosity using the 2–50 keV flux of the source as a measure of the bolometric flux and they normalized this quantity by a value of  $L_{\text{Edd}} = 2.5 \times 10^{38}$  erg s $^{-1}$ , which corresponds to the Eddington luminosity of a  $1.9 M_{\odot}$  neutron star accreting matter with cosmic abundance (the same method was used in Jonker et al. 2001). The distances used to calculate the luminosity and the corresponding references are listed in table 1 in Ford et al. (2000).

More modern estimates of the distance to our sources (see e.g. Kuulkers et al. 2003, 2010; Galloway et al. 2008; Arnason et al. 2021) are in agreement within errors with the distances used by Ford et al. (2000). For the error of the luminosity, we considered two factors: First, for each source, the distribution of the intensity when the lower kHz QPO is present has a spread of 10–30 per cent of the average value (e.g. Méndez et al. 2001; Barret, Olive & Miller 2007; Barret, Bouteiller & Miller 2008). Second, the error of the luminosity reflects the error in the estimate of the distance to these sources. While distances given in the literature have an accuracy of  $\sim 50$  per cent, the values obtained using different methods have a spread of  $\sim 20$  per cent, much smaller than the errors of the individual measurements (for a detailed discussion of these and other potential sources of error of the luminosity, see Méndez 2006). Given the above, here we use a fixed error of 25 per cent for  $L/L_{\text{Edd}}$ . The luminosity of each source in our sample and its error is listed in Table 2.

## 3 RESULTS

In Table 1 we show the data we obtained from Troyer et al. (2018). The best fitting slope,  $m$ , and intercept,  $c$ , in the table are taken from Troyer et al. (2018), who fitted a linear relation to the energy-

**Table 1.** Slope,  $m$ , and intercept,  $c$ , of the best-fitting linear function to the time-lag energy spectra of the lower and upper kHz QPOs as given by Troyer et al. (2018). Slope,  $\alpha_1$ , below the break of the best-fitting broken-line function to the fractional rms energy spectra of the lower kHz QPO in fig. 4 in Troyer et al. (2018). Total fractional rms amplitude between 2 and 25 keV,  $\text{rms}_{2-25 \text{ keV}}$ , of both the lower and upper kHz QPOs. For the broken-line fit to the fractional rms energy spectra of the lower kHz QPO, we fixed  $\alpha_2$ , the slope above the break, to zero and linked the break energy to be the same for all sources, with a best-fitting value  $E_{\text{break}} = 10.3 \pm 0.2$  keV. The slope  $m$  is shown here with changed signs with respect to the values given by Troyer et al. (2018) as we considered the linear model fitted to the data to be  $\Delta t(E) = -mE + c$ .

Source	Lower kHz QPO				Upper kHz QPO		
	$m$ ( $\mu\text{s keV}^{-1}$ )	$c$ ( $\mu\text{s}$ )	$\alpha_1$ (per cent $\text{keV}^{-1}$ )	$\text{rms}_{2-25 \text{ keV}}$ (per cent)	$m$ ( $\mu\text{s keV}^{-1}$ )	$c$ ( $\mu\text{s}$ )	$\text{rms}_{2-25 \text{ keV}}$ (per cent)
4U 0614+09	$8.1 \pm 1.0$	$54.4 \pm 4.9$	$1.17 \pm 0.03$	$10.34 \pm 0.25$	$0.5 \pm 1.1$	$2.3 \pm 5.5$	$10.2 \pm 0.4$
4U 1702-43	$6.4 \pm 0.7$	$52.9 \pm 3.2$	$0.97 \pm 0.02$	$8.57 \pm 0.16$	$5.7 \pm 2.3$	$44.8 \pm 8.7$	$8.83 \pm 1.05$
Aql X-1	$5.6 \pm 0.7$	$42.5 \pm 3.3$	$0.90 \pm 0.02$	$7.91 \pm 0.17$			
4U 1608-52	$4.9 \pm 0.6$	$37.3 \pm 2.6$	$1.01 \pm 0.02$	$8.94 \pm 0.14$	$2.3 \pm 1.2$	$15.0 \pm 5.4$	$10.3 \pm 0.7$
4U 1915-05	$4.0 \pm 3.7$	$35.4 \pm 16.7$	$1.0 \pm 0.2$	$8.76 \pm 1.34$			
4U 1636-53	$3.2 \pm 0.3$	$24.3 \pm 1.3$	$0.91 \pm 0.01$	$8.03 \pm 0.11$	$-0.63 \pm 0.57$	$-5.0 \pm 2.0$	$9.6 \pm 0.3$
4U 1728-34	$2.2 \pm 0.4$	$20.3 \pm 1.4$	$0.80 \pm 0.01$	$6.99 \pm 0.12$	$-0.8 \pm 0.3$	$-7.2 \pm 1.3$	$8.3 \pm 0.2$
EXO 1745-248	$1.5 \pm 1.1$	$11.6 \pm 4.1$	$0.90 \pm 0.05$	$7.83 \pm 0.37$			
4U 1820-30	$1.1 \pm 0.4$	$8.9 \pm 1.7$	$0.54 \pm 0.02$	$4.74 \pm 0.12$	$1.1 \pm 1.7$	$10.1 \pm 7.0$	$4.7 \pm 0.4$
4U 1735-44	$0.9 \pm 0.5$	$8.1 \pm 1.8$	$0.73 \pm 0.02$	$6.42 \pm 0.15$			
XTE J1739-285	$0.5 \pm 1.5$	$4.0 \pm 5.9$	$0.95 \pm 0.08$	$8.37 \pm 0.58$			
SAX J1748.9-202	$0.4 \pm 3.6$	$-20.4 \pm 12.4$	$1.2 \pm 0.2$	$10.39 \pm 1.26$			
IGR J17191-2821	$0.08 \pm 1.41$	$2.7 \pm 5.2$	$0.91 \pm 0.07$	$8.00 \pm 0.47$			
4U 1705-44	$-6.5 \pm 3.9$	$-54.5 \pm 17.9$	$0.55 \pm 0.08$	$4.86 \pm 0.58$			

**Table 2.** Luminosities in Eddington units for the eight sources in our sub-sample selected from Troyer et al. (2018). References: (1) Ford et al. (2000); (2) Jonker et al. (2001).

Source	$l = L/L_{\text{Edd}}$	Reference
4U 0614 + 09	$0.065 \pm 0.016$	1
4U 1702-43	$0.046 \pm 0.018$	2
Aql X-1	$0.015 \pm 0.041$	1
4U 1608-52	$0.030 \pm 0.075$	1
4U 1636-53	$0.085 \pm 0.021$	1
4U 1728-34	$0.070 \pm 0.017$	1
4U 1820-30	$0.20 \pm 0.05$	1
4U 1735-44	$0.12 \pm 0.03$	1

dependent time lags<sup>1</sup> in figs 8 and 9,  $\Delta t(E)$  versus energy,  $\Delta t(E) = -mE + c$ . The sources in Table 1 are sorted on the basis of this best-fitting slope  $m$ . We also show in Table 1 the total fractional rms amplitude integrated from 2 to 25 keV for both the lower and upper kHz QPOs and the best-fitting parameters of a broken-line model fit we performed to the fractional rms amplitude of the lower kHz QPO as a function of energy (see fig. 4 in Troyer et al. 2018), with slopes  $\alpha_1$  and  $\alpha_2$ , below and above the break energy,  $E_{\text{break}}$ , respectively. Because for some sources  $E_{\text{break}}$  and  $\alpha_1$  and/or  $\alpha_2$  were not well constrained (e.g. 4U 1915-05, SAX J1748.9-202 and 4U 1705-44), while in all cases the slope above the break was consistent with zero within errors, in the fit we fixed  $\alpha_2$  to zero and linked  $E_{\text{break}}$  to be the same for all sources.

From Table 1, it is apparent that the slope below the break energy of the fractional rms amplitude fit generally decreases as the slope of the lag spectrum decreases. If we consider only the sub-sample of eight sources with data over the full QPO frequency range, for which we have obtained luminosities from the literature (listed in Table 2), it is apparent that as the luminosity increases the slope of the fractional

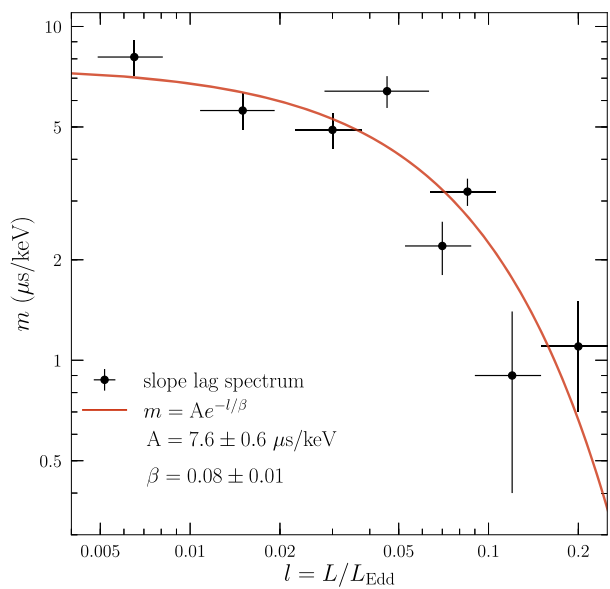


**Figure 1.** Slope of the time-lag spectrum,  $m$  (taken from Troyer et al. 2018), of the lower kHz QPO versus luminosity in Eddington units for the eight sources in Table 2. The red solid line indicates the best-fitting exponential model to the data (see text).

rms spectrum and that of the time-lag spectrum decrease, indicating that both quantities depend upon luminosity.

To explore this, in Fig. 1 we plot the slope of the time-lag spectrum (from Table 1) of the lower kHz QPO versus luminosity for the eight sources in our sub-sample (see Table 2). The solid red line in the figure corresponds to the best-fitting exponential model,  $m = A e^{-l/\beta}$  where  $l = L/L_{\text{Edd}}$ , to the data, with  $A = 7.6 \pm 0.6 \mu\text{s keV}^{-1}$  and  $\beta = 0.08 \pm 0.01$ . In this figure it is apparent that as the luminosity increases the slope in the time-lag spectrum decreases exponentially. The same behaviour can be observed in Fig. 2, where we plot the total fractional rms amplitude integrated from 2 to 25 keV of the lower

<sup>1</sup> Since most slopes in Troyer et al. (2018) are negative, here we reversed the sign of the slope in the linear relation so that most of the slopes are positive.

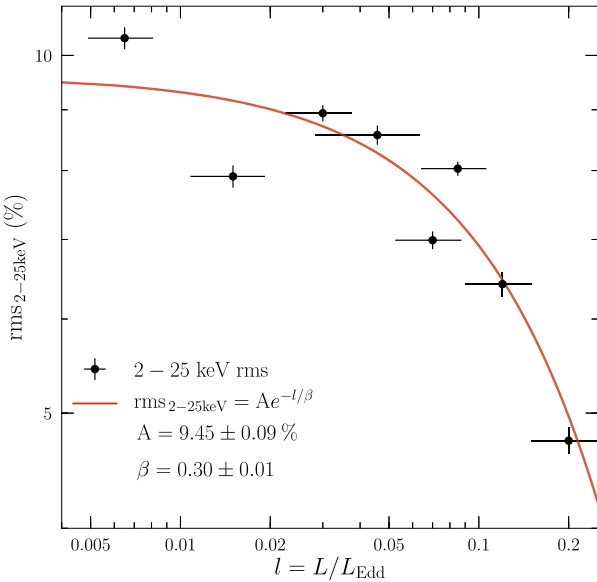


**Figure 2.** Total fractional rms amplitude, between 2 and 25 keV, of the lower kHz QPO versus luminosity for the eight sources in Table 2. The red solid line indicates the best-fitting exponential model to the data (see text).

kHz QPO versus luminosity for the same sub-sample of sources. Like in Fig. 1, the solid red line corresponds to the best-fitting exponential model to the data,  $\text{rms}_{2-25\text{keV}} = Ae^{-l/\beta}$ , with values  $A = 9.45 \pm 0.09$  per cent and  $\beta = 0.30 \pm 0.01$ . As in the case of the slope of the time-lag spectrum, the total 2–25 keV rms amplitude also decreases exponentially with the luminosity of the source.

Although we do not show it here, the average lag between two broad energy bands (see values in Troyer et al. 2018, tables 2 and 3) and the slope below the break of the rms spectrum (see values in Table 1) of the lower kHz QPO behave in the same way when plotted versus the luminosity of the source, with those quantities also decreasing exponentially with increasing luminosity.

We performed a similar analysis for the relations of the slope of the time-lag spectrum and the total fractional rms amplitude upon luminosity on the six sources of Troyer et al. (2018) where they observed the presence of the upper kHz QPOs (see Table 1). In Fig. 3, we show the slope of the time-lag spectrum of the upper kHz QPO versus luminosity, with the red solid line showing the best-fitting exponential model,  $m = Ae^{-l/\beta}$ , to the data. Due to the time lags being less well constrained for the upper than the lower kHz QPO, we performed a joint fit of the exponential model on the time-lag slope data of both the lower and the upper kHz QPOs. In this joint fit we linked  $\beta$  to be the same for both data sets, as these parameters were consistent with each other in an independent fit. The resulting best-fitting parameters for the joint model are  $A = 1.2 \pm 0.5 \mu\text{s keV}^{-1}$  and  $\beta = 0.08 \pm 0.01$ . Because the value of  $A$  in this model is consistent with zero at  $2.2\sigma$ , we performed an  $F$ -test to determine whether a model with  $A$  free would be favoured over a model with  $A$  fixed to zero. The  $F$ -test probability is 0.5, which means that the slope of the time-lag spectrum of the upper kHz QPO is consistent with zero. In Fig. 4, we show the total fractional rms amplitude of the upper kHz QPO versus luminosity. Here we fit again an exponential model,  $\text{rms}_{2-25\text{keV}} = Ae^{-l/\beta}$ , jointly to both the lower and upper kHz QPOs data sets with  $\beta$  linked. The best-fitting parameters resulting from the joint fit are  $A = 10.8 \pm 0.02$  per cent and  $\beta = 0.30 \pm 0.01$ . As is the case for the lower kHz QPO, here the total fractional rms amplitude also decreases exponentially with increasing luminosity.

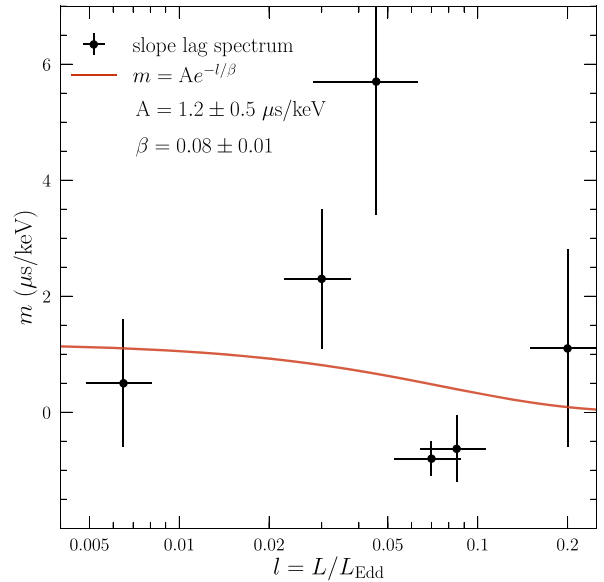


**Figure 3.** Slope of the time-lag spectrum,  $m$  (taken from Troyer et al. 2018), of the upper kHz QPO versus luminosity in Eddington units for the six sources in Table 2 that show upper kHz QPOs. The red solid line indicates the best-fitting exponential model to the data (see text).

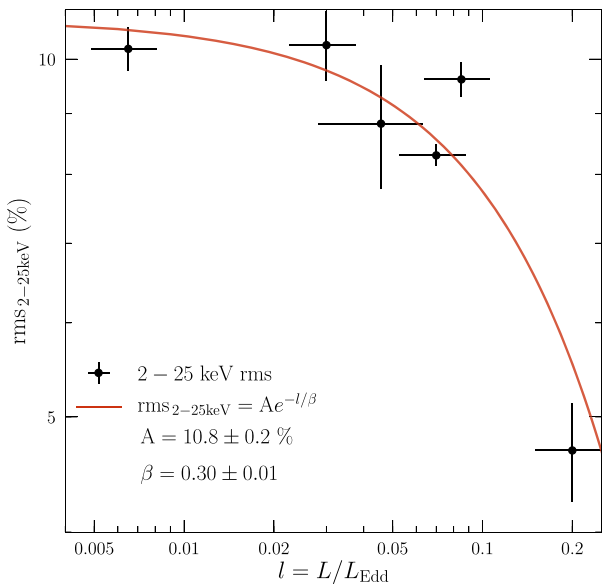


**Figure 4.** Total fractional rms amplitude, between 2 and 25 keV, of the upper kHz QPO versus luminosity for the six sources in Table 2 that show upper kHz QPOs. The red solid line indicates the best-fitting exponential model to the data (see text).

Since both the fractional rms amplitude and the slope of the time-lag energy spectrum of the lower kHz QPO correlate with luminosity in a similar fashion, in Fig. 5 we plot these quantities together for the same sub-sample of sources in Figs 1 and 2. The red solid line in the figure corresponds to the best-fitting linear model,  $m = a \times \text{rms}_{2-25\text{keV}} + b$ , with  $a = 1.1 \pm 0.3 \mu\text{s (keV per cent)}^{-1}$  and  $b = -4.8 \pm 2.1 \mu\text{s keV}^{-1}$ . From this figure, it is apparent that there is a

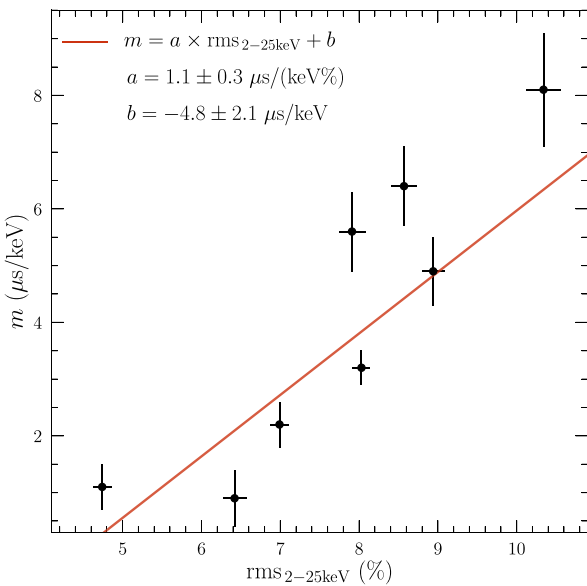


**Figure 5.** Slope of the time lag,  $m$ , versus the total fractional rms amplitude, between 2 and 25 keV, of the lower kHz QPO for the eight sources in Table 2. The red solid line indicates the best-fitting linear model to the data (see text).

strong linear correlation between the slope of the time-lag spectrum and the total rms amplitude of the sources. Not shown here, there are similar strong correlations between the broad-band lag and both the total 2–25 keV rms amplitude and the slope below the break of the rms spectrum.

#### 4 DISCUSSION

We discovered that, as with the rms fractional amplitude, the energy-dependent time lags of the lower kHz QPOs depend upon luminosity in eight neutron-star LMXBs. Indeed we showed, for the first time, that the slope of the time-lag spectrum of the lower kHz QPO decreases exponentially with increasing luminosity. Since the fractional rms amplitude of the lower kHz QPO also decreases exponentially with luminosity, it follows that the slope of the time-lag spectra increases linearly with the average rms amplitude of the lower kHz QPO. For the upper kHz QPOs detected in six of the eight neutron-star LMXBs we studied, the fractional rms amplitude decreases exponentially with luminosity, while the slope of the time-lag spectrum is consistent with zero.

The lags of the lower kHz QPOs are soft, meaning that the variability in the soft band is lagging behind that in the hard band. High-energy X-ray photons reflected off an accretion disc have been observed to produce soft lags, known as reverberation lags, in black-hole LMXBs (see Uttley et al. 2014, for a review of reverberation in accreting black holes). Particularly for neutron-star systems, Cackett (2016) studied the soft lags of the lower kHz QPO in 4U 1608–52 and explored the possibility that the lags were due to reverberation (Barret 2013). Cackett (2016) showed that the lag spectrum should increase with energy above 8 keV if reverberation is the sole mechanism responsible for the soft lags of the lower kHz QPO in 4U 1608–52. Observations show the opposite trend, suggesting that reverberation is not the mechanism producing the soft lags of the lower kHz QPOs in 4U 1608–52; by extension, the same must be true for the lower kHz QPOs in the other sources in this paper. It is worth mentioning that Coughenour et al. (2020) performed a similar study of the lags

of the upper kHz QPO in the source 4U 1728–34, finding that reverberation alone cannot be responsible for those lags either.

To make the case stronger against the accretion disc being directly responsible for the soft lags we observe in these sources, we can consider the behaviour of the fractional rms amplitude for the 14 sources in fig. 4 in Troyer et al. (2018). The fractional rms amplitude of the kHz QPOs in these 14 sources increases with energy up to 10 keV, reaching values of 10–12 per cent at  $\sim$ 20 keV (see also Berger et al. 1996; Gilfanov, Revnivtsev & Molkov 2003; Ribeiro et al. 2019, where similar results are shown). At these energies, the spectrum of a neutron-star LMXB is dominated by the emission of a Comptonizing component or corona (Sunyaev & Titarchuk 1980; White, Stella & Parmar 1988), while the contribution of the accretion disc is negligible, suggesting that the corona must be responsible for the amplitude and the lag spectra of the lower kHz QPOs (Sanna et al. 2010).

Inverse Compton scattering in the corona, as the electrons transfer energy to the soft photons coming from the accretion disc or the surface of the neutron star, produces a time delay of the hard photons with respect to the directly emitted soft photons (Wijers, van Paradijs & Lewin 1987; Lee & Miller 1998). Inverse Compton scattering would therefore produce only hard lags, in conflict with the observations of soft lags in our data. However, if we consider Comptonization as proposed by Lee et al. (2001), Kumar & Misra (2016), and Karpouzas et al. (2020), we can explain the observed soft lags accounting for feedback occurring between the corona and the accretion disc. In this scenario, a fraction of the Comptonized photons impinge back on to the accretion disc, where they are thermalized and emitted at later times and lower energies than the photons coming from the corona. Since this effect produces another time delay, now for the soft photons that returned to the disc, we would observe soft lags, which is what we find in the data (see Kumar & Misra 2014; Karpouzas et al. 2020).

In Fig. 5, both the total rms amplitude and the slope of the time-lag energy spectrum of the lower kHz QPO are shown to be linearly correlated with each other, as they both decrease in a similar manner with increasing luminosity. This trend suggests that there is a single property of the system that drives the changes we observe in the rms amplitude and the time lags of the kHz QPOs. The dependence upon luminosity could imply that the trends we see in Figs 1, 2, and 4 are determined by changes in the corona, as the sources become softer due to a smaller coronal contribution to the total energy spectrum with increasing luminosity. At low luminosities, for example, the accretion rate decreases and the energy spectrum becomes hard; the corona is then optically thin and the amplitude of the variability increases. In this scenario, the properties of the corona drive the properties of the variability, as it occurs in the Compton up-scattering model we described in the previous paragraph.

As we explained in Section 2, the luminosity of the source can change significantly (by a factor of  $\sim$ 1.5–5 depending on the source) when the lower kHz QPO is present; the spread, however, is  $\sim$ 10–30 per cent of the average luminosity. On the other hand, when the lower kHz QPO is present the hard colour of the source changes by less than  $\sim$ 5–10 per cent peak to peak (see e.g. figs 2 and 6 in Barret et al. 2007), whereas at the vertex of the colour–colour diagram, when the lower kHz QPO is present, the average hard colour of these sources changes by a factor of  $\sim$ 2 (see e.g. van Straaten et al. 2000; Zhang, Méndez & Altamirano 2011; García, Zhang & Méndez 2013; Zhang et al. 2017). If the hard colour is a proxy of the properties of the corona, the above considerations show that the change of the average properties of the corona from source to source is significantly larger than the change within a single source when the lower kHz QPO

is present. Since the hard colour and luminosity of neutron-star X-ray binaries are correlated (van Paradijs & van der Klis 1994), it is appropriate to take the luminosity as a proxy for the properties of the corona.

To further understand the dependence of the properties of the kHz QPOs upon the properties of the corona, we can examine what happens with the quality factor as a function of the frequency of the QPO and the luminosity of the source. Similar to the fractional rms amplitude, the quality factor of the lower kHz QPO increases and then decreases with QPO frequency (see e.g. Di Salvo, Méndez & van der Klis 2003; Barret, Olive & Miller 2005a) and with increasing luminosity (see e.g. Méndez 2006). The fact that the quality factor, the fractional rms amplitude, and the time lags of the lower kHz QPO depend upon luminosity suggests that there is a coupled mode of oscillation between the corona and the disc. Lee et al. (2001) proposed that this mode is responsible for the lower kHz QPO, which would arise from a resonance between oscillations in the disc (or the neutron star surface) and the corona (see e.g. de Avellar et al. 2013, 2016; Ribeiro et al. 2017, 2019; Zhang et al. 2017). The frequency at which the quality factor and the rms amplitude of the QPO peak would correspond to a natural frequency of the corona depends upon its properties. At high luminosities, the contribution of the corona to the energy spectrum of a source and the feedback to the disc decreases, and the oscillations of both the disc and the corona are not in resonance, leading to a decrease of the rms amplitude, quality factor, and lags.

The nature of the oscillation mode we believe to be responsible for the variability we observe in the emission of the neutron-star LMXBs in our sample, and the behaviour of the timing properties of the QPOs, is uncertain. To better comprehend what drives this oscillation resonance, we can consider the work of Karpouzas et al. (2020), based on the model in Kumar & Misra (2014), where they conceive the QPO as a small oscillation in the solution of the Kompaneets equation, that describes the evolution of the energy spectrum of the source dominated by inverse Compton scattering (Kompaneets 1957). The model in Karpouzas et al. (2020) links the behaviour of the timing properties of the QPO to the physical quantities accounted for in the Kompaneets equation, e.g. the electron temperature and size of the corona. Karpouzas et al. (2020) fit their model to both the rms and lag spectra of the lower kHz QPO in 4U 1636–53 and find that the perturbations in coronal properties are the ones producing the oscillations in the emission of the source, reaching their maximum variability at a QPO frequency of 700 Hz. These results suggest that the corona is responsible for the dependence upon QPO frequency of the lag and the fractional rms amplitude of the lower kHz QPO, and hint at the existence of a resonance between the source of the soft photons and the corona. This conclusion agrees with what we find in this paper: the luminosity of the source is related to properties of the corona, like its temperature, optical depth, and size, that together with the feedback fraction of photons that return to the soft-photon source can explain the energy-dependent fractional rms amplitude and time lags of the lower kHz QPOs (see section 2 in Karpouzas et al. 2020, for a more detailed explanation of the model).

Compton up-scattering model of Lee et al. (2001) could also explain the difference between the properties of the time lag of the lower and upper kHz QPOs (see Figs 1 and 3, and Table 1), due to the dependence upon frequency of the resonance between the disc and the corona. In neutron-star LMXBs, the coexistence between the soft lags of the lower kHz QPOs and the hard lags of the upper kHz QPOs (see e.g. de Avellar et al. 2013; Peille et al. 2015) can be expected, because the oscillations of the coronal properties depend on QPO frequency in this Compton up-scattering model. Similarly, the

presence of other features, like the hard lags of the BBN component that remain roughly independent of frequency in the range between  $\sim 0.01$  and  $\sim 100$  Hz (see e.g. Miyamoto et al. 1988; Ford et al. 1999), could also be predicted by the model.

In the context of the scenario that we described in this section, the neutron-star LMXB XTE J1701–462 becomes a unique case to study, as it is one of only two sources to show atoll-like and Z-like<sup>2</sup> behaviour during the same outburst (Homan et al. 2007; Lin, Remillard & Homan 2009; Homan et al. 2010). Sanna et al. (2010) studied the kHz QPOs in XTE J1701–462, in both the atoll and Z phases, and found that the maximum quality factor and the maximum rms amplitude of the lower kHz QPOs of both phases follow the same trend with luminosity that Méndez (2006) described for other neutron-star LMXBs (see fig. 5 in Sanna et al. 2010). The results presented here suggest that the time-lag energy spectrum of the lower kHz QPO in the two different phases of XTE J1701–462 will change with luminosity in a similar way to what we show in Fig. 1. Such a relation, if observed, would help to further understand the nature of the mechanism responsible for the lower kHz QPO in neutron-star LMXBs, isolating the changes in the system that luminosity depends upon other factors like the mass of the neutron star, the inclination of the accretion disc, or the strength of the magnetic field.

## ACKNOWLEDGEMENTS

The authors wish to thank Federico García and Konstantinos Karpouzas for useful discussions that helped with the ideas presented in this manuscript. They also thank the referee for insightful comments that helped improve the clarity of the paper. This research has made use of data obtained from the High Energy Astrophysics Science Archive Research Center, provided by NASA’s Goddard Space Flight Center.

## DATA AVAILABILITY

The data underlying this article are publicly available at the website of the High Energy Astrophysics Science Archive Research Center (<https://heasarc.gsfc.nasa.gov/>).

## REFERENCES

- Altamirano D., van der Klis M., Méndez M., Wijnands R., Markwardt C., Swank J., 2008, *ApJ*, 687, 488
- Arnason R. M., Papie H., Barmby P., Bahramian A., Gorski M. D., 2021, *MNRAS*, 502, 5455
- Barret D., 2013, *ApJ*, 770, 9
- Barret D., Olive J.-F., Miller M. C., 2005a, *Astron. Nachr.*, 326, 808
- Barret D., Olive J.-F., Miller M. C., 2005b, *MNRAS*, 361, 855
- Barret D., Olive J.-F., Miller M. C., 2006, *MNRAS*, 370, 1140
- Barret D., Olive J.-F., Miller M. C., 2007, *MNRAS*, 376, 1139
- Barret D., Boutelier M., Miller M. C., 2008, *MNRAS*, 384, 1519
- Belloni T., Psaltis D., Klis M. v. d., 2002, *ApJ*, 572, 392
- Berger M., van der Klis M., 1998, *A&A*, 340, 143
- Berger M. et al., 1996, *ApJ*, 469, L13
- Bradt H. V., Rothschild R. E., Swank J. H., 1993, *A&AS*, 97, 355
- Cackett E. M., 2016, *ApJ*, 826, 103
- Coughenour B. M., Cackett E. M., Peille P., Troyer J. S., 2020, *ApJ*, 889, 136
- de Avellar M. G. B., Méndez M., Sanna A., Horvath J. E., 2013, *MNRAS*, 433, 3453

<sup>2</sup>Neutron-star LMXBs are usually divided into two categories, atoll and Z, depending on the pattern they describe during an outburst in their colour–colour diagram (Hasinger & van der Klis 1989).

de Avellar M. G. B., Méndez M., Altamirano D., Sanna A., Zhang G., 2016, *MNRAS*, 461, 79

Di Salvo T., Méndez M., van der Klis M., Ford E., Robba N. R., 2001, *ApJ*, 546, 1107

Di Salvo T., Méndez M., van der Klis M., 2003, *A&A*, 406, 177

Ford E. C., van der Klis M., Méndez M., van Paradijs J., Kaaret P., 1999, *ApJ*, 512, L31

Ford E. C., van der Klis M., Méndez M., Wijnands R., Homan J., Jonker P. G., van Paradijs J., 2000, *ApJ*, 537, 368

Galloway D. K., Muno M. P., Hartman J. M., Psaltis D., Chakrabarty D., 2008, *ApJS*, 179, 360

García F., Zhang G., Méndez M., 2013, *MNRAS*, 429, 3266

Gilfanov M., Revnivtsev M., Molkov S., 2003, *A&A*, 410, 217

Grove J. E. et al., 1994. Fichtel C. E., Gehrels N., Norris J. P., eds, *AIP Conf. Proc. Vol. 304, The Second Compton Symposium*, Am. Inst. Phys., p. 192

Hasinger G., van der Klis M., 1989, *A&A*, 225, 79

Homan J. et al., 2007, *ApJ*, 656, 420

Homan J. et al., 2010, *ApJ*, 719, 201

Jahoda K., Swank J. H., Giles A. B., Stark M. J., Strohmayer T., Zhang W., Morgan E. H., 1996, *Proc. SPIE Vol. 2808, EUV, X-Ray, and Gamma-Ray Instrumentation for Astronomy VII*. SPIE, Bellingham, p. 59

Jonker P. G. et al., 2001, *ApJ*, 553, 335

Kaaret P., Piraino S., Ford E. C., Santangelo A., 1999, *ApJ*, 514, L31

Karpouzas K., Méndez M., Ribeiro E. M., Altamirano D., Blaes O., García F., 2020, *MNRAS*, 492, 1399

Kluzniak W., Abramowicz M. A., 2001, preprint (astro-ph/0105057)

Kompaneets A. S., 1957, Sov. J. Exp. Theor. Phys., 4, 730

Kumar N., Misra R., 2014, *MNRAS*, 445, 2818

Kumar N., Misra R., 2016, *MNRAS*, 461, 2580

Kuulkers E., den Hartog P. R., in't Zand J. J. M., Verbunt F. W. M., Harris W. E., Cocchi M., 2003, *A&A*, 399, 663

Kuulkers E. et al., 2010, *A&A*, 514, A65

Lee H. C., Miller G. S., 1998, *MNRAS*, 299, 479

Lee H. C., Misra R., Taam R. E., 2001, *ApJ*, 549, L229

Lin D., Remillard R. A., Homan J., 2009, *ApJ*, 696, 1257

Méndez M., 2006, *MNRAS*, 371, 1925

Méndez M., Belloni T. M., 2020, High-Frequency Variability in Neutron-Star Low-Mass X-ray Binaries. Astrophysics and Space Science Library, 461, p. 263

Méndez M. et al., 1998, *ApJ*, 494, L65

Méndez M., van der Klis M., Ford E. C., 2001, *ApJ*, 561, 1016

Miller M. C., Lamb F. K., Psaltis D., 1998a, *ApJ*, 508, 791

Miller M. C., Lamb F. K., Cook G. B., 1998b, *ApJ*, 509, 793

Miyamoto S., Kitamoto S., Mitsuda K., Dotani T., 1988, *Nature*, 336, 450

Miyamoto S., Kimura K., Kitamoto S., Dotani T., Ebisawa K., 1991, *ApJ*, 383, 784

Morgan E. H., Remillard R. A., Greiner J., 1997, *ApJ*, 482, 993

Nowak M. A., 2000, *MNRAS*, 318, 361

Osherovich V., Titarchuk L., 1999, *ApJ*, 522, L113

Peille P., Barret D., Uttley P., 2015, *ApJ*, 811, 109

Pottschmidt K. et al., 2003, *A&A*, 407, 1039

Psaltis D., 2008, *Living Rev. Relativ.*, 11, 9

Ribeiro E. M., Méndez M., Zhang G., Sanna A., 2017, *MNRAS*, 471, 1208

Ribeiro E. M., Méndez M., de Avellar M. G. B., Zhang G., Karpouzas K., 2019, *MNRAS*, 489, 4980

Sanna A. et al., 2010, *MNRAS*, 408, 622

Stella L., Vietri M., 1997, *ApJ*, 492, L59

Strohmayer T. E., 2001, *ApJ*, 552, L49

Strohmayer T. E., Zhang W., Swank J. H., Smale A., Titarchuk L., Day C., Lee U., 1996, *ApJ*, 469, L9

Sunyaev R. A., Titarchuk L. G., 1980, *A&A*, 500, 167

Titarchuk L., 2003, *ApJ*, 591, 354

Troyer J., Cackett E., Peille P., Barret D., 2018, *ApJ*, 860, 167

Uttley P., Cackett E. M., Fabian A. C., Kara E., Wilkins D. R., 2014, *A&AR*, 22, 72

van Paradijs J., van der Klis M., 1994, *A&A*, 281, L17

van Straaten S., Ford E. C., van der Klis M., Méndez M., Kaaret P., 2000, *ApJ*, 540, 1049

van Straaten S., van der Klis M., di Salvo T., Belloni T., Psaltis D., 2002, *ApJ*, 568, 912

van der Klis M., 2005, *Astron. Nachr.*, 326, 798

van der Klis M., Swank J. H., Zhang W., Jahoda K., Morgan E. H., Lewin W. H. G., Vaughan B., Paradijs J. v., 1996, *ApJ*, 469, L1

Vaughan B. A. et al., 1997, *ApJ*, 483, L115

White N. E., Stella L., Parmar A. N., 1988, *ApJ*, 324, 363

Wijers R. A. M. J., van Paradijs J., Lewin W. H. G., 1987, *MNRAS*, 228, 17P

Zhang G., Méndez M., Altamirano D., 2011, *MNRAS*, 413, 1913

Zhang G., Méndez M., Sanna A., Ribeiro E. M., Gelfand J. D., 2017, *MNRAS*, 465, 5003

This paper has been typeset from a TeX/LaTeX file prepared by the author.